Comparisons of sets of electron–neutral scattering cross sections and swarm parameters in noble gases: III. Krypton and xenon

Article *in* Journal of Physics D Applied Physics · August 2013

DOI: 10.1088/0022-3727/46/33/334003

CITATIONS
16

READS
530

10 authors, including:

M. C. Bordage
Paul Sabatier University - Toulouse III
55 PUBLICATIONS **1,031** CITATIONS
SEE PROFILE

Stephen Biagi
University of Liverpool
217 PUBLICATIONS **5,097** CITATIONS
SEE PROFILE

L.L. Alves
Technical University of Lisbon
130 PUBLICATIONS **1,185** CITATIONS
SEE PROFILE

L. C. Pitchford
165 PUBLICATIONS **5,455** CITATIONS
SEE PROFILE

Comparisons of sets of electron–neutral scattering cross sections and swarm parameters in noble gases: III. Krypton and xenon

2013 J. Phys. D: Appl. Phys. 46 334003

(http://iopscience.iop.org/0022-3727/46/33/334003)

J. Phys. D: Appl. Phys. **46** (2013) 334003 (16pp) doi:10.1088/0022-3727/46/33/334003

Comparisons of sets of electron–neutral scattering cross sections and swarm parameters in noble gases: III. Krypton and xenon

M C Bordage[1,2], S F Biagi[3], L L Alves[4], K Bartschat[5], S Chowdhury[1], L C Pitchford[1,2], G J M Hagelaar[1,2], W L Morgan[6], V Puech[7] and O Zatsarinny[5]

[1] Université de Toulouse; UPS, INPT; LAPLACE (Laboratoire Plasma et Conversion d'Energie); 118 route de Narbonne, F-31062 Toulouse cedex 9, France
[2] CNRS; LAPLACE; F-31062 Toulouse, France
[3] Oliver Lodge Laboratory, University of Liverpool, Oxford St., Liverpool L69 7ZE, UK
[4] Instituto de Plasmas e Fusão Nuclear, Instituto Superior Técnico, Universidade Técnica de Lisboa, Av. Rovisco Pais, 1049-001 Lisboa, Portugal
[5] Department of Physics and Astronomy, Drake University, Des Moines, IA 50311, USA
[6] Kinema Research and Software, PO Box 1146, Monument, CO 80132, USA
[7] Laboratoire de Physique des Gaz et des Plasmas, CNRS et Univ. Paris-Sud F-91405, Orsay, France

E-mail: marie-claude.bordage@laplace.univ-tlse.fr

Received 26 April 2013, in final form 20 June 2013
Published 5 August 2013
Online at stacks.iop.org/JPhysD/46/334003

Abstract
This paper, the third in a series of three, describes work carried in the context of Plasma Data Exchange Project of the Gaseous Electronics Conference (PDEP-GEC) to compare electron collision cross-sections sets from ground-state, noble gases atoms and to check their consistency with measured swarm parameters. Such consistency is a minimum requirement if the cross-section data are to be used for modelling low-temperature plasmas. In this paper, we present intercomparisons of the independently compiled sets of electron cross-sections from ground-state, neutral Kr and Xe atoms presently available on the LXCat open-access website (www.lxcat.laplace.univ-tlse.fr). Swarm parameters (reduced mobility, characteristic energy, reduced longitudinal diffusion coefficient, reduced ionization coefficient) calculated in a Boltzmann solver or Monte Carlo simulation using these cross-sections sets are compared with experimental data, also available online on the LXCat site.

(Some figures may appear in colour only in the online journal)

1. Introduction

The purpose of this paper is to document data available on the LXCat open-access site, www.lxcat.laplace.univ-tlse.fr, for xenon and krypton for electron scattering cross-sections and for transport and ionization coefficients. Xenon is used in a number of applications areas from light sources to x-ray detectors for imaging medicine, border security and high-energy particle physics (Santos *et al* 1991). Low-temperature plasmas in xenon-containing gas mixtures generated in dielectric barrier discharges are used for industrial applications such as plasma display panels, pollution control, surface treatment, decontamination and sterilization (Kogelschatz *et al* 1997, Laroussi *et al* 2002, Boeuf 2003, Becker *et al* 2005). Electron scattering cross-sections in xenon have been of interest for many years for modelling, for example, excimer lasers and other UV light sources (Rhodes 1979, Sosnin *et al* 2006). Because of these many applications in fields related to low-temperature plasmas, there is a large body of data on electron scattering cross-sections and swarm parameters in Xe, whereas data for Kr are more limited.

The type of data required for modelling the electron component of the plasma depends on the level of modelling:

for kinetic models, microscopic scattering cross-sections for all the collisional processes are required, whereas for fluid models, macroscopic quantities—transport and rate coefficient, for example—are the required input parameters. The link between cross-sections and calculated transport and rate coefficients is provided by the Boltzmann equation which can be solved to obtain the electron energy distribution function (eedf) and then macroscopic quantities can be calculated by appropriately averaging over the eedf. In situations where there is a local balance between the energy gained by electrons in the electric field and the energy lost in collisions with the neutral gas, the transport and rate coefficients are functions of the reduced electric field strength, E/N, the ratio of the electric field strength to the neutral density. Transport and rate coefficients measured in such conditions are 'swarm parameters' and these data provide extremely useful points for checking the consistency of cross-section datasets used as input to the Boltzmann solver. Cross section datasets should be consistent with swarm data before being used in plasma modelling for more complex (non-stationary, non-local) situations. We provide those checks here for the cross section datasets for Kr and Xe available on the LXCat site.

The present paper (paper III) like the two companion papers (referred to paper I for argon (Pitchford *et al* 2013) and paper II for helium and neon (Alves *et al* 2013)) report comparisons of independently compiled sets of cross sections for electron scattering with neutral krypton and xenon atoms in their ground-states. We also report comparisons of swarm data calculated using the cross sections sets and check the consistency of results obtained against measurements available. The energy range of interest is thermal up to about 1 keV. An overview of theoretical methods for calculations of electron–atom scattering cross sections is presented in another paper (paper IV) (Bartschat 2013) in this cluster issue.

The cross section datasets presently available on LXCat for krypton and xenon come mainly from an iterative procedure based on adjustment of cross sections until the calculated swarm parameters are in agreement with measurements. For more details, see papers I and II. Other datasets are based on the recent quantum calculations (Zatsarinny and Bartschat 2010, Allan *et al* 2011, Zatsarinny *et al* 2011) which provide differential scattering cross sections in Kr and Xe for elastic and inelastic collisions (but not yet for ionization). From the differential cross sections, the total scattering cross sections for excitation can be deduced, as well as the elastic momentum transfer cross section. These are the quantities used as input data in standard two-term Boltzmann solvers to yield the eedf (see appendix J of paper I).

This work was originally reported at the 2011 Gaseous Electronic Conference (GEC) and was inspired by the GEC Plasma Data Exchange Project (PDEP) (Bordage *et al* 2011). The GEC Plasma Data Exchange Project is an informal, community-based project which was initiated as a result of a public discussion held at the 2010 Gaseous Electronics Conference (GEC), a major international meeting for the low-temperature plasma community. This project aims to address, at least in part, the well-recognized needs for the community to organize the means of collecting, evaluating and sharing data both for modelling and for interpretation of experiments.

This paper is organized as follows: section 2 is devoted to a presentation of the cross sections sets available on LXCat website for krypton and xenon. Intercomparisons of the most relevant cross sections are presented. These datasets are used to calculate swarm parameters with a Boltzmann solver and a Monte Carlo simulation. Section 3 is dedicated to the comparison of calculated and experimental values of electron swarm parameters (reduced mobility, ratio of the mobility to the longitudinal and the transverse diffusion coefficients, and reduced ionization coefficient). Conclusions are given in section 4. The appendices, written by individual contributors/co-authors, contain additional information and comments about how the cross sections sets were assembled and how they should be used.

2. Comparisons of cross sections in krypton and xenon presently available in the LXCat databases

At present there are five sets of cross sections for electron scattering in krypton and seven sets for xenon. The sets all contain cross sections for elastic momentum transfer $Q_{\mathrm{m,el}}$, for total ionization Q_{i} (except for the BSR datasets), and for excitation to various excited states. The cross sections differ considerably in the detail included for the inelastic processes, ranging from two effective excitation levels in the MORGAN databases (for both xenon and krypton) to a detailed description of up to 74 levels (BSR for xenon) for cross sections for individual excitation processes from the ground state.

The cross section sets of Zatsarinny and Bartschat for xenon (Zatsarinny and Bartschat 2010) and krypton (Hoffmann *et al* 2010, Zatsarinny and Bartschat 2010, Allan *et al* 2011) result directly from quantum calculations using the Dirac B-Spline R-Matrix method (DBSR) and provide detailed information about the structure in the near threshold region for the main excitation processes. However, these datasets must be completed by the addition of total ionization cross sections before being used in a Boltzmann solver or in Monte Carlo simulations. The calculations reported below and labeled 'BSR+' correspond to results obtained using as input the elastic momentum transfer and excitation cross sections from the BSR datasets and the total ionization cross section from Rapp and Englander-Golden (1965). Such a procedure provides a preliminary consistency check of the BSR data in Kr and Xe, but it is not conclusive. Note that theoretical ionization cross sections are included in the BSR datasets for Ar and Ne, as discussed in papers I and II.

The BIAGI-v7.1, BIAGI-v8.9, HAYASHI, MORGAN, and PUECH cross section sets have been compiled through an iterative process—collecting cross sections from the literature, evaluating swarm parameters, comparing with experimental swarm data, adjusting if necessary the magnitudes of the cross sections to improve the agreement between calculated and measured swarm data. The resulting cross sections sets should be complete (in the sense that the major electron momentum and energy loss processes are included) and consistent with experimental swarm data. Comparisons should be made for a maximum number of parameters over a wide range of E/N, but even if good agreement is found for all comparisons,

it is still not possible to determine a unique cross section dataset in this way. Additional constraints can be imposed on cross sections, but uniqueness remains an elusive goal. Nevertheless, consistency with swarm data is a minimum requirement for cross section datasets to be useful for plasma modelling. The SIGLO datasets are based on Date *et al* (1989) for Kr and in part on Puech and Mizzi (1991) for Xe, but with different groupings of excited states. Checks were made to confirm that swarm parameters are adequately predicted by these datasets, but no effort was made to adjust the SIGLO datasets to achieve better agreement with swarm parameters.

The LXCat website (www.lxcat.laplace.univ-tlse.fr) is structured into databases (Panchnesnyi *et al* 2011) provided by individual contributors, each database containing sets of cross sections for different target gas species, such as ground-state krypton and xenon. The cross sections considered in this paper were downloaded from the LXCat between August and December 2012.

Table 1 provides a list of all the databases presently available on LXCat containing datasets for krypton and xenon. The database name in the first column of the table and the level of description of the cross section set is in the second column. The third column gives the name of the contributors and how the cross sections were determined. When the compilations of cross sections are well-documented in the literature, references are given in the table. This is the case for the xenon datasets from the HAYASHI and PUECH databases and for the Kr and Xe datasets in the BSR database. The other datasets have been described only partially in the literature or not at all. More details about how they were derived and tested and on how they should be used are given in the appendices.

Users are requested to provide the references given in the table in all publications making use of these data and to cite the LXCat website (www.lxcat.laplace.univ-tlse.fr). Users are further requested to cite the sources of original data (see appendices) where possible.

The older databases (BIAGI-v7.1, MORGAN and SIGLO) for krypton and (BIAGI-v7.1, HAYASHI, MORGAN, PUECH and SIGLO) for xenon include a limited number of excitation levels (between 2 and 14). The number of excitation cross sections in the recent (since 2010) cross sections datasets of both BIAGI-v8.9 and BSR is larger than 50.

Figures 1 to 6 (1, 3 and 5 for krypton and 2, 4 and 6 for xenon) show comparisons of the cross sections, from the different databases. Like argon, krypton and xenon have a Ramsauer–Townsend minimum in their elastic cross section at low energy (around 0.65 eV for xenon and 0.54 eV for krypton).

Figure 1 for krypton and figure 2 for xenon present the elastic momentum transfer cross sections, $Q_{\mathrm{m,el}}$, from the different swarm-derived compilation sets, along with the calculated elastic momentum transfer and total elastic scattering $Q_{\mathrm{T,el}}$ from BSR. Although we do not use $Q_{\mathrm{T,el}}$ in the Boltzmann calculations, it is useful to see these two quantities determined from the elastic differential cross sections given from the quantum calculations of Zatsarinny and Bartschat.

The other compilations on LXCat do not include $Q_{\mathrm{T,el}}$. Note that in some applications (e.g. plasma electron beam and radiation dose absorption calculations (Kowari *et al* 1989, Waibel and Grosswendt 1991), the use of the total elastic cross section is necessary. Modern treatments of the radiation dose absorption in electron or particle beams use the ratio of the total elastic to momentum transfer cross section, with knowledge of these two cross sections the angular distribution in scattering are calculated from algorithm proposed by Okhrimovskyy *et al* (2002).

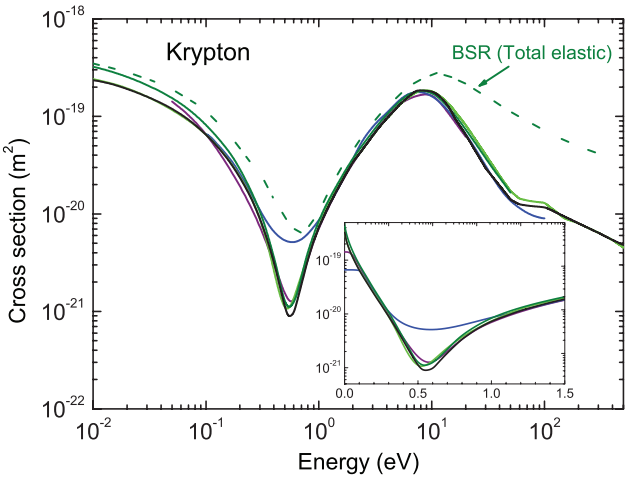

Figure 1. Comparisons of elastic momentum transfer cross section versus electron energy in krypton from the different databases. The inset is a zoom in the region of the Ramsauer minimum. The color code is the same for all figures in this paper: BIAGI-v8.9 (——); BIAGI-v7.1 (——); BSR (——); SIGLO (——); MORGAN (——).

There is reasonable agreement among the different datasets for the elastic momentum cross sections in krypton and in xenon. The location and the amplitude of the Ramsauer–Townsend minimum is the same for the different datasets, including the BSR quantum calculations, except for SIGLO in krypton and SIGLO and PUECH in xenon where the depth of the minima is higher than in the other datasets. A zoom of the region near the Ramsauer–Townsend minimum is presented in the insets in figure 1 for krypton and figure 2 for xenon. For krypton, the position of the minimum is within 20% and, except for SIGLO, the differences in the depth are 30% or less. For xenon, the SIGLO cross section was taken from PUECH, and the BIAGI-v7.1 and v8.9 are identical below the onset of the inelastic channels. The agreement among the datasets is better in xenon than in krypton.

In the 2–20 eV region and in the region of the maximum, the agreement is quite good (except for MORGAN in xenon where the data are limited to 5 eV and below). This region plays an important role in the calculations of the drift velocity for $E/N > 1$ Td (the unit Townsend, Td $= 10^{-21}$ V m^2). Increasing differences in the $Q_{\mathrm{m,el}}$ between the datasets appear after the maximum. The structure at high energy for quantum calculations (BSR) in xenon is also observed in the swarm-derived cross sections set of HAYASHI, but this has no effect on the calculated swarm parameters because, in this region, inelastic processes are dominant.

Comparisons of the cross sections with each dataset for total (summed) excitation and for ionization are illustrated in figure 3, for krypton and in figure 4 for xenon. A zoom of the

Table 1. List of databases on LXCat for electron–krypton and electron–xenon scattering cross sections. The first column is the name of the database (given by the contributors), the second column is a summary of the contents of the dataset, and the third column gives the names of contributors, references, key data and how the cross sections were determined. More details about the individual datasets are given in the appendices as indicated.

Database name	Level of description for krypton and xenon	Comments
BIAGI-v7.1	Krypton: 4 cross sections Elastic, Ionization, 3 excitation levels (grouped into S, P and D&P levels) Xenon: 6 cross sections Elastic, Ionization, 4 excitation levels	Contributor: SF Biagi. (See appendix A) Reference: BIAGI-v7.1 database, www.lxcat.laplace.univ-tlse.fr; Transcribed from SF Biagi's Fortran code MAGBOLTZ, Version 7.1, 2004. http://consult.cern.ch/writeup/magboltz Swarm-derived cross section set developed using Monte Carlo simulations.
BIAGI-v8.9	Krypton: 53 Cross sections Elastic, Ionization, 51 excitation levels Xenon: 52 Cross sections Elastic, Ionization, 50 excitation levels	Contributor: SF Biagi. (See appendix A) Reference: BIAGI-v8.9 database, www.lxcat.laplace.univ-tlse.fr; Transcribed from SF Biagi's Fortran code MAGBOLTZ,Version 8.97, 2011. http://consult.cern.ch/writeup/magboltz Swarm-derived cross section set developed using Monte Carlo simulations.
BSR	Krypton: 69 Cross sections Elastic, 68 excitation levels Xenon: 75 Cross sections Elastic, 74 excitation levels	Contributors: O Zatsarinny and K Bartschat (See appendix B) Reference: BSR database, www.lxcat.laplace.univ-tlse.fr Kr References: Zatsarinny and Bartschat (2010); Allan *et al* (2011); Zatsarinny *et al* (2011) Xe Reference: Zatsarinny and Bartschat (2010) Theoretical calculations using Dirac B-Spline R-matrix (DBSR) method. Ionization cross section is not included. All calculations identified as 'BSR+' in the text were performed using the BSR datasets for Kr or Xe, with the addition of the total cross section for ionization from Rapp and Englander-Golden (1965).
HAYASHI	Xenon: 16 Cross sections Elastic, Ionization, 14 excitation levels	Uploaded to the HAYASHI database by the LXCat team at LAPLACE, Toulouse; (See appendix C). Reference: HAYASHI database, www.lxcat.laplace.univ-tlse.fr (Hayashi 2003) Swarm-derived cross section set developed using Monte Carlo simulations.
MORGAN	Krypton: 4 Cross sections Elastic, Ionization, 2 excitation levels (metastable + resonance) Xenon: 4 Cross sections Elastic, Ionization, 2 excitation levels (metastable + resonance)	Contributor: WL Morgan (See appendix E paper I) Reference: MORGAN database, www.lxcat.laplace.univ-tlse.fr These data were compiled over 30 years ago by WL Morgan and were available for many years on the Kinema Software website. Swarm-derived cross section set developed using the two-term Boltzmann solver, ELENDIF (Morgan and Penetrante 1990). Xe: The MORGAN database has been widely used in the community, and so we include it here in the comparisons even though we do not recommend it for use with BOLSIG+ because of the limited energy range (up to only 5 eV) for elastic momentum transfer cross section, $Q_{\mathrm{m,el}}$.
PUECH	Xenon: 15 Cross sections Elastic, Ionization, 13 excitation levels	Contributor: V. Puech (See appendix D) Reference: PUECH database, www.lxcat.laplace.univ-tlse.fr; Puech and Mizzi (1991) Swarm-derived cross section set developed using a multi-term Boltzmann solver (Segur *et al* (1986).
SIGLO	Krypton: 7 Cross sections Elastic, Ionization, 5 excitation levels Xenon: 8 Cross sections Elastic, Ionization, 6 excitation levels	Contributor: GREPHE Group, LAPLACE, Toulouse (See appendix E) Reference: SIGLO database, www.lxcat.laplace.univ-tlse.fr Kr: Data digitized from Date *et al* (1989) Xe: Meunier *et al* (1995), and based on Puech and Mizzi (1991). For Kr, this is a swarm-derived cross section set, developed by Date *et al* (1989) using a two-term Boltzmann solver. The data for Kr on LXCat were digitized from the above reference and distributed for use with BOLSIG+ (Hagelaar and Pitchford 2005). In the course of this work, we re-digitized the data and uploaded revised data to LXCat in November 2012. Swarm parameters calculated with these revised data are in better agreement with experiment than the results shown in the original reference.

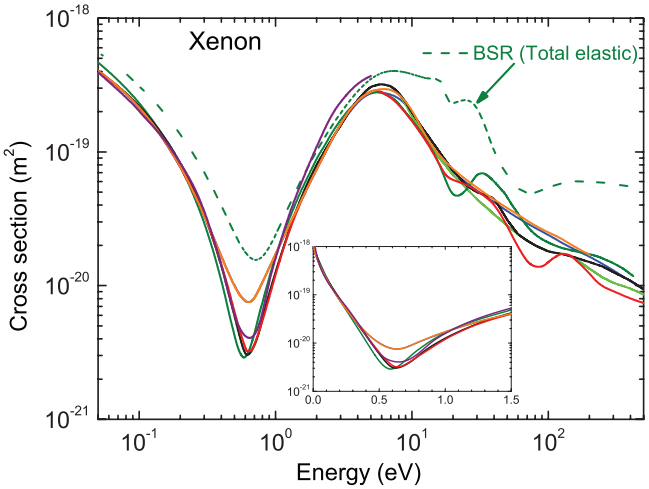

Figure 2. Comparisons of elastic momentum transfer cross section versus electron energy in xenon from the different databases. The inset is a zoom in the region of the Ramsauer minimum. The color code is the same for all figures in this paper: BIAGI-v8.9 (——); BIAGI-v7.1 (——); BSR (——); HAYASHI (——); SIGLO (——); MORGAN (——); PUECH (——).

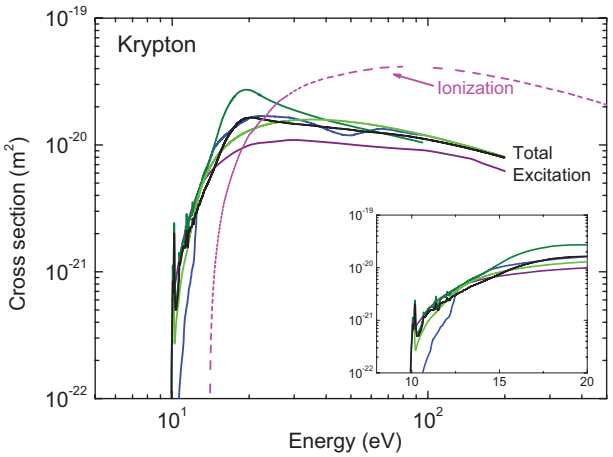

Figure 3. Total excitation and ionization cross sections versus electron energy in krypton from the different databases. The inset is a zoom between 8 and 20 eV to show the near-threshold resonance structures. The color code is: BIAGI-v8.9 (——); BIAGI-v7.1 (——); BSR (——); SIGLO (——); MORGAN (——). For ionization: Rapp and Englander-Golden (1965) (- - - -).

low-energy region near the threshold is shown in the insets of these figures, to enhance the detail in the resonance region and up to 20 eV.

The total excitation cross section is the only way to compare the inelastic cross sections among the various datasets, which differ in how the excited states are grouped together. The ionization cross section in all datasets for xenon and krypton is taken from Rapp and Englander-Golden (1965), except for the BIAGI datasets (see detailed comments in appendix A), and PUECH (Xe) who took into account the more recent measured ionization cross section of Wetzel *et al* (1987) (figures 3 and 4). The differences are very slight.

Significant differences appear for the total excitation cross section from one database to another, for both the energy dependence and the magnitude.

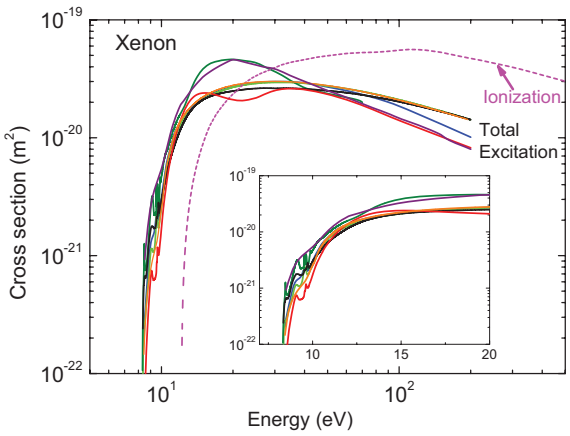

Figure 4. Total excitation and ionization cross sections versus electron energy in xenon from the different databases. The inset is a zoom between 8 and 20 eV to show the near-threshold resonance structures. The color code is: BIAGI-v8.9 (——); BIAGI-v7.1 (——); BSR (——); HAYASHI (——); SIGLO (——); MORGAN (——); PUECH (——). For ionization : Rapp and Englander-Golden (1965) (- - - -).

The inelastic cross sections are provided for energies up to 150 eV in the quantum calculations of Zatsarinny and Bartschat for krypton and to 80 eV for xenon. The total inelastic cross sections in BSR for xenon and krypton around 20 eV are significantly higher than in the other compilations (except for the MORGAN xenon dataset), and this is mainly due to the neglect of coupling to the ionization continuum in the calculations. The present BSR models are optimized for the energy region near the low-lying thresholds, which is dominated by negative ion resonances. More details are given in appendix B.

At low energy, near threshold, the energy dependence and the magnitude of total excitation cross sections the BSR dataset exhibits resonance structures. For BIAGI-v8.9, as mentioned in appendix A, and in order to capture the resonance structures, the BSR results were used with a small scaling factor to better fit the ionization coefficient. The scaling factor was within the experimental uncertainty of the Allan *et al* cross section measurements. For the other databases, the structure in the resonance region is not resolved.

To show the different contributions to the total inelastic cross sections, we plot in figure 5 for krypton and figure 6 for xenon the excitation cross sections for the sum of the two metastable levels ($1s_5 + 1s_3$), the two resonance levels ($1s_4 + 1s_2$), the ten 2p levels ($2p_{10}$ to $2p_1$) and the other remaining levels (sum of all excitation levels except metastable, resonant and 2p), for the different datasets considered. The same energy range is used for all the figures (up to 100 eV). Table 2 gives complementary information about these levels.

Sufficient detail for such comparisons for krypton is provided in the databases of BIAGI v8.9, BSR and in part in SIGLO. The cross sections in the BIAGI-v7.1 and MORGAN datasets are more global and cannot be separated into excitation of specific levels.

Among the seven datasets for xenon, we can compare the different contributions from BIAGI-v8.9 and BSR. The level grouping in the PUECH dataset precludes separating

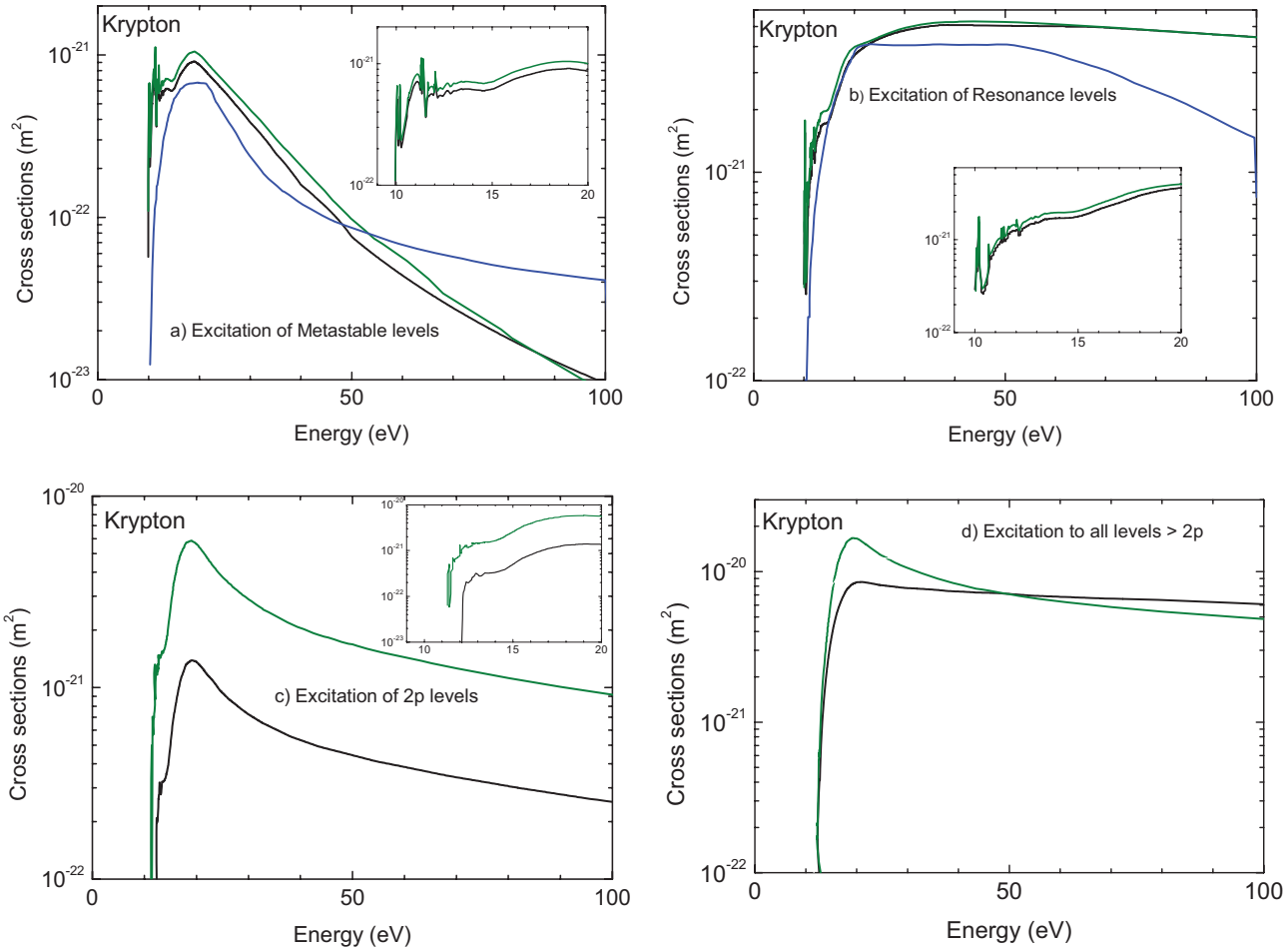

Figure 5. Comparisons of cross sections in krypton versus electron energy for (*a*) summed excitation of metastable levels (*b*) summed excitation of resonance levels (*c*) summed excitation of all 2p levels; and (*d*) sum of all remaining excitation. The color code is: BIAGI-v8.9 (——); BSR (——); SIGLO (——).

the sum of cross sections for excitation to 2p levels from the sum of all other higher excitation. The BIAGI-v7.1, MORGAN, HAYASHI and SIGLO datasets are not included in this comparison because of their different groupings of levels. In the MORGAN dataset, there are only two excitation cross sections, and four in BIAGI-v7.1. In SIGLO, one cross section groups the resonant states and some of the 2p levels. In the HAYASHI dataset, the $2p_{10}$ and $2s_2$ levels are grouped in one cross section and the sum of the cross sections of the 2p levels is limited to $2p_9$ to $2p_6$.

The cross sections plotted in figures 5 and 6 for krypton and xenon should show the correct behaviour as a function of energy: dipole allowed resonance levels, which decay to the ground state, should exhibit a fall-off approximately as $\log(\varepsilon)/\varepsilon$ at high energy, where ε is energy; the forbidden levels, i.e. those that cannot decay to the ground state by dipole emission, fall off with energy at a faster rate that depends on the extent to which the transition is forbidden. The BIAGI-v8.9 datasets for krypton and xenon reflect this behaviour.

The cross sections datasets presented here are complete and can be used directly in two-term or multi-term (or Monte Carlo) Boltzmann solvers. Information about the numerical methods used to calculate swarm parameters from the cross sections can be found in appendix J of paper I.

In the two-term Boltzmann solver used here, BOLSIG+, cross sections are assumed to depend on $\log(\varepsilon)/\varepsilon$ for the purpose of extrapolation to energies higher than those given in the data tables. While this is not a good approximation for the elastic momentum transfer cross section, most of the datasets do go to sufficiently high energies so that there is no effect of this extrapolation. Notable exceptions are the MORGAN datasets for Kr and Xe. The highest energy in the tables for $Q_{\mathrm{m,el}}$ is 20 eV for Kr and 5 eV for Xe. Especially in the latter this limits the accuracy of the predicted swarm parameters, as discussed in section 3.1. Unless otherwise indicated, linear interpolation is used to find values of the cross sections between entries provided in the data tables.

3. Comparisons of swarm data

The list of calculated swarm data is the same as the list presented in other companion papers, except for the reduced excitation coefficients (see table 3 for definition, symbols and units). All swarm data are functions of the reduced electric field strength E/N, where E is the electric field strength and N the neutral gas density.

Calculations are performed using the freeware package, BOLSIG+, which is a Boltzmann solver based on the two-term

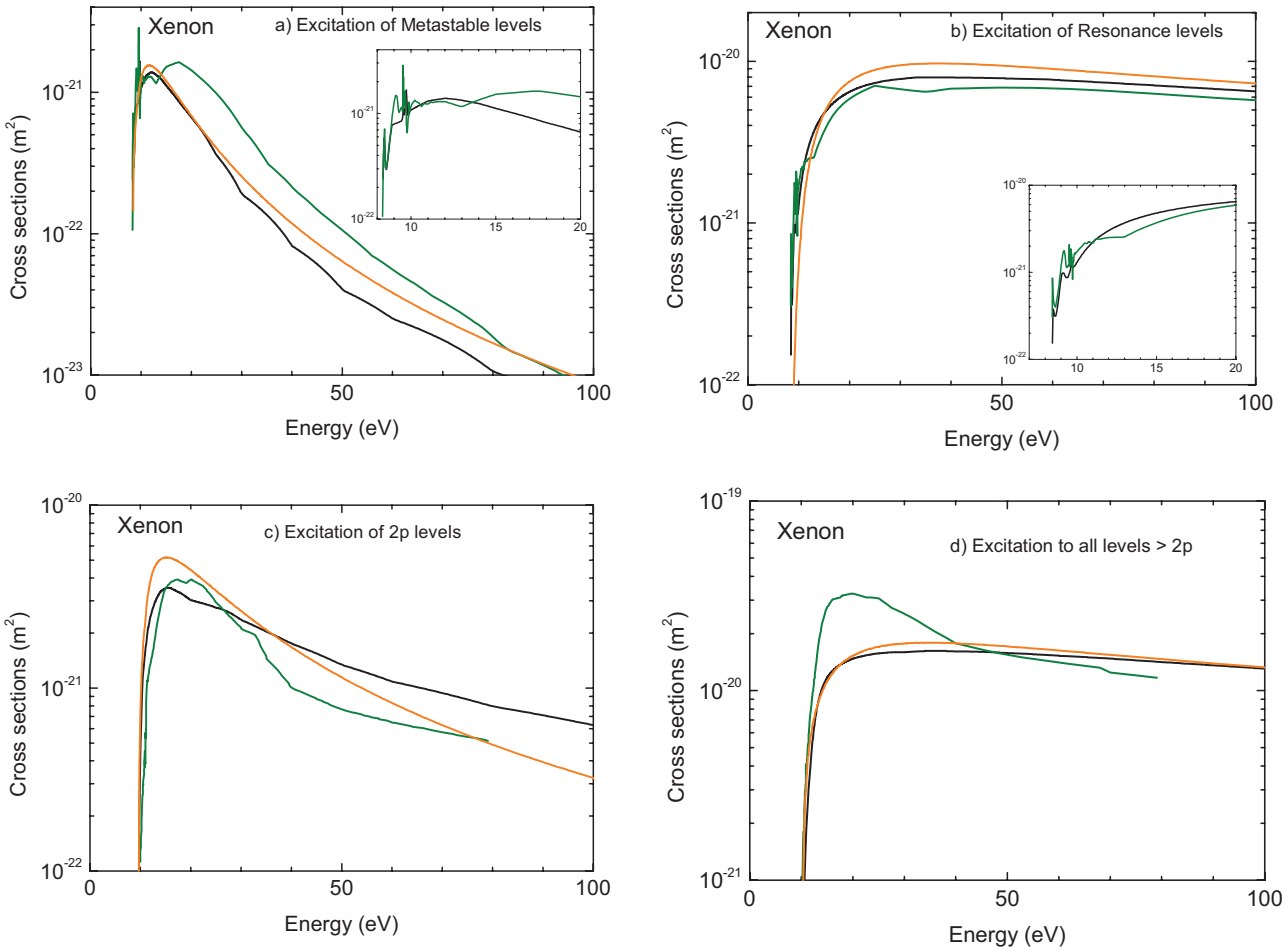

Figure 6. Comparisons of cross sections in xenon versus electron energy for (*a*) summed excitation of metastable levels (*b*) summed excitation of resonance levels (*c*) summed excitation of all 2p levels; and (*d*) sum of all remaining excitation. The color code is: BIAGI-v8.9 (——); BSR (——); PUECH (——).

Table 2. Paschen notation, Racah and LS designations, and energy threshold of the lowest excitation levels in krypton and xenon (Kramida *et al* 2013).

	Krypton			Xenon		
Level name Paschen	Racah	LS	Energy(eV)	Racah	LS	Energy(eV)
Metastable levels						
$1s_5$	$5s[3/2]_2$	$^3P_2$	9.9152	$6s[3/2]_2$	$^3P_2$	8.315
$1s_3$	$5s'[1/2]_0$	$^3P_0$	10.562	$6s'[1/2]_0$	$^3P_0$	9.447
Resonance levels						
$1s_4$	$5s[3/2]_1$	$^3P_1$	10.032	$6s[3/2]_1$	$^3P_1$	8.437
$1s_2$	$5s'[1/2]_1$	$^1P_1$	10.644	$6s'[1/2]_1$	$^1P_1$	9.570
2p levels						
$2p_{10}$ ...	$5p[1/2]_1$		11.303	$6p[1/2]_1$		9.580
$2p_1$	$5p'[1/2]_0$		12.256	$6p'[1/2]_0$		11.141

approximation (Hagelaar and Pitchford 2005). We used the default energy grid and convergence criteria and assuming equal sharing of energy among the two electrons exiting the ionization events. For the most part, the spatial growth model (or steady state Townsend, SST) was used for calculations of μN, D_T/μ and α_i/N and the temporal growth model (or pulsed Townsend, PT) was used for the calculation of $D_L N$ and D_L/μ (longitudinal diffusion cannot be measured in SST experiments, see appendix J, paper I for details). The calculations are realized over a wide E/N range, typically between 10^{-3} and 1000 Td. Note that the choice of growth model has no effect for low E/N where the electron number density is constant. At 200 Td, μN and α_i/N calculated using SST and PT models differ by some 5% and 10%, and the differences increase to 10% and 15% for the highest values of E/N shown in the curves below for both Kr and Xe.

To confirm results from two-term calculations, the determination of the swarm parameters from Monte Carlo

Table 3. List of swarm parameters discussed here with symbols and units.

Parameter	Symbol	units
Reduced electron mobility	μN (μ is the mobility and N is the neutral gas number density).	$(\mathrm{m\,V\,s})^{-1}$
Density normalized transverse diffusion coefficient	$N D_\mathrm{L}$	$(\mathrm{m\,s})^{-1}$
Ratio of transverse diffusion coefficient to mobility	D_T/μ	V
Characteristic energy	$u_k = eD_\mathrm{T}/\mu$ (e is the electronic charge)	eV
Density normalized longitudinal diffusion coefficient	$N D_\mathrm{L}$	$(\mathrm{m\,s})^{-1}$
Ratio of longitudinal diffusion coefficient to mobility	D_L/μ	V
Reduced Townsend (or ionization) coefficient	α_i/N	m^2

Table 4. List of experimental databases available on LXCat with interest for krypton and xenon.

Database name	Contents
DUTTON	Transcription of data from J Dutton, 'Survey of Electron Swarm Data', (Dutton 1975)
LAPLACE	Data published after or not appearing in the 1975 Dutton review. These data were assembled at LAPLACE in Toulouse, France, are relatively complete for noble and simple atmospheric gases, and additional data are being uploaded regularly. When possible, data were taken from published tables.

Table 5. List of experimental data chosen for krypton and xenon.

Swarm parameter	References	
	Kr	Xe
μN	Nakamura (1990) Hunter *et al* (1988) Kücükarpaci and Lucas (1981) Pack *et al* (1992)	Šašić *et al* (2005) Hunter *et al* (1988) Hashimoto and Nakamura (1990)
D_T/μ	Koizumi *et al* (1986) Al-Amin and Lucas (1987)	Koizumi *et al* (1986) Kobayashi *et al* (2006) Kobayashi *et al* (2004)
D_L/μ	Pack *et al* (1992) Nakamura (1990)	Pack *et al* (1992) Hashimoto and Nakamura (1990)
α_i/N	Kruithof (1940) Heylen (1971) Specht *et al* (1980) Jacques *et al* (1986)	Kruithof (1940) Bhattacharya (1976) Jacques *et al* (1986) Specht *et al* (1980)

simulation were performed using MAGBOLTZ (Biagi 2011) and MCIG, an independently developed Monte Carlo simulation (Hagelaar 2012). A number of checks were made to insure that both codes gave identical results. The multi-term Boltzmann solver developed by Ségur *et al* (1984) was also used to evaluate the accuracy of the two-term results.

Experimental data are also available on LXCat. For krypton and xenon they come from the two databases listed in table 4.

Table 5 lists the experimental data for krypton and xenon for each swarm parameter that we have selected for the comparisons.

We have selected only a few of the available data on the LXCat website for comparison with calculated values of the swarm parameters. The choice was mainly guided by the purity of the gas (see appendix I, paper I), following the criteria for selection of experimental data to be used for comparison. Calculations made with only 0.01% of N_2 show differences in the reduced mobility of more than 10% for $E/N = 1$ Td in Xe and a little bit lower for Kr (8% at the same E/N value). Since the experimental data of Kücükarpaci and Lucas (1981) are the only ones at high E/N (> 100 Td) in krypton, we include these data even though they do not strictly fit the criteria elaborated in appendix I of Paper I. For the same reason, the values of D_T/μ obtained by Al-Amin and Lucas (1987) were also taken into account.

Note that Nakamura (1990) for krypton and Hashimoto and Nakamura (1990) for xenon measure $N D_\mathrm{L}$. In the same experiments, the authors measured drift velocities (reduced mobility μN) that we used in converting the original $N D_\mathrm{L}$ data to D_L/μ for the comparisons here.

All measurements and calculations presented in this paper are obtained at gas temperature $T_\mathrm{g} = 300$ K.

3.1. Comparison of measured and calculated drift velocity (reduced mobility)

The experimental values of the reduced mobility μN (converted from the original measurements of the drift velocity which span more orders of magnitude, using $v_\mathrm{d} = \mu N \times E/N$) are compared to BOLSIG+ calculations. Results are shown in figure 7 for krypton and in figure 8 for xenon. The insets in the figures are zooms to illustrate the differences among calculations and with measurements, in the 1 to 1000 Td E/N region.

The depth of the Ramsauer minimum has only a small effect on the low field mobility but may affect the transverse diffusion. Because the mobility above about 3 Td is sensitive to variations in the inelastic cross sections, the considerable spread reported in the excitation cross sections close to threshold (e.g. see figure 4 for xenon) in the various datasets, leads to the observed differences in the calculated mobilities in the region of the knee in the curve around 3 Td.

In krypton, both BSR and MORGAN have an elastic momentum transfer cross section larger than BIAGI at the

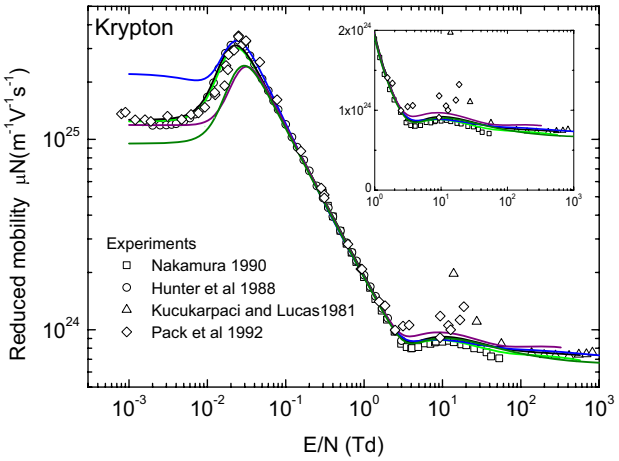

Figure 7. Measured and calculated reduced electron mobility versus E/N in krypton. The symbols are experimental data referenced in the table 5 and the solid lines are calculations using a two-term Boltzmann solver. The inset is a zoom to illustrate the differences in the results in the 1 to 1000 Td region. The color code is: BIAGI-v8.9 (——); BIAGI-v7.1 (——); BSR+ (——); SIGLO (——); MORGAN (——).

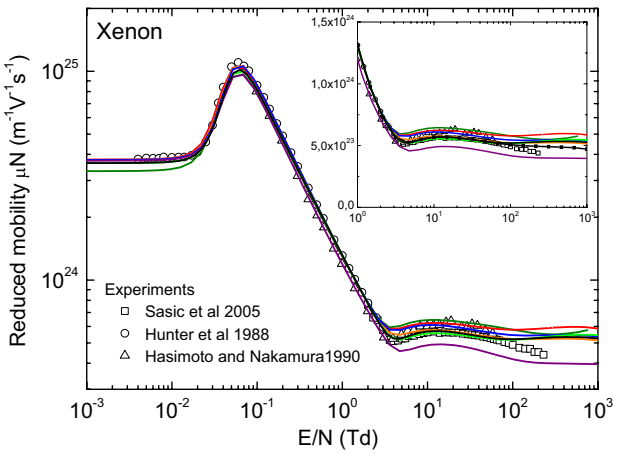

Figure 8. Measured and calculated reduced electron mobility versus E/N in xenon. The symbols are experimental data referenced in the text (table 5) and the solid lines are calculations using a two-term Boltzmann solver. The inset is a zoom to illustrate the differences in the results in the [1–1000 Td] E/N region for which PT calculations with BIAGI-v8.9 (-■-) are added. The color code is: BIAGI-v8.9 (——); BIAGI-v7.1 (——); BSR+ (——); HAYASHI (——); SIGLO (——); MORGAN (——); PUECH (——).

lowest energies in figure 1, and this explains the differences observed in the mobilities calculated with these datasets at the lowest values of E/N and near their maximum values around 0.03 Td. SIGLO's μN is too high at very low E/N (<0.02 Td) compared to experiments, which suggests that its $Q_{\mathrm{m,el}}$ at very low energy is too low. As seen in the inset in figure 1, it is indeed about a factor of 6 lower than values in the other datasets, possibly due to uncertainties introduced during the digitization of the original data from Date *et al* (1989). The BIAGI-v8.9 and BIAGI-v7.1 datasets give essentially the same predictions for the reduced mobility for E/N up to about 100 Td. Calculations for $E/N > 0.1$ Td using the SIGLO database overlap with those using BIAGI-v8.9, which are in good agreement with experiment over the full range of E/N, although there is considerable scatter in the selected data between 10 and 100 Td. Except for the higher (>100 Td) and the lower (<0.1 Td) values of E/N, the BSR+ dataset (theoretical elastic momentum transfer and excitation cross sections complemented by the ionization cross section from Rapp and Englander-Golden (1965)) yields results in excellent agreement with measurements. Calculations using the MORGAN dataset do not reproduce the selected experimental data as well as the others, but these measurements were published several years after the MORGAN dataset was compiled. The Nakamura data are the most accurate of the experimental data between 1 and 40 Td. The measurement was done with a variable length drift tube to remove end effects and gave excellent accuracy in the better known gas argon. The divergence of the Nakamura data with the Pack *et al* (1992) and Kücükarpaci and Lucas (1981) data is likely to be caused by the decreased accuracy of these measurements. The latter two experiments were optimized for accurate measurements at electric fields below 1 Td for the Pack *et al* data and above 100 Td for the Kücükarpaci and Lucas data.

As seen in figure 8, there is more of a spread in the calculated results for reduced mobility using the different datasets in xenon than in krypton. This is in spite of the fact that relatively more information is available about electron scattering cross sections in xenon, as mentioned in the introduction. All calculations are in good agreement among themselves and with experiment for low E/N and until the knee in the curve at about 3 Td. Thereafter, the measurements we have selected for comparisons differ among themselves (by up to 10% in the 10 to 50 Td range) more than with the calculations, if we exclude MORGAN from the comparisons. The MORGAN elastic momentum transfer cross section is limited to 5 eV in xenon and the sum of its inelastic cross sections is not in good agreement with the other datasets (see figure 4). Thus it is not surprising that the MORGAN results for the reduced mobility deviate considerably from the measurements for E/N greater than a few Td. And, as mentioned above, the calculations reported here were done using the default extrapolation scheme in BOLSIG+, $\log(\varepsilon)/\varepsilon$, where ε is the electron energy, which is not really appropriate for elastic momentum transfer cross sections (Phelps and Pitchford 1985). The two BIAGI datasets and the PUECH dataset yield results in good agreement with the most recent measurements of Šašić *et al* (2005) up to almost 100 Td, and the SIGLO and HAYASHI datasets are in good agreement with the measurements of Hasimoto and Nakamura (1990). None of the datasets predict the decrease in mobility observed in the experiments of Šašić *et al* for $E/N > 100$ Td when used with BOLSIG+ or with Monte Carlo. Note that the experiments were performed using a Pulsed Townsend (PT) set-up and so a more proper comparison of calculations with these experiments should take this into account for $E/N > 100$ Td. The inset in figure 8 shows the detail of the 1 to 1000 Td region and includes an additional curve calculated using the PT growth model with cross sections from BIAGI-v8.9. While the agreement with the Šašić *et al* is improved, as expected, there remains a noticeable difference

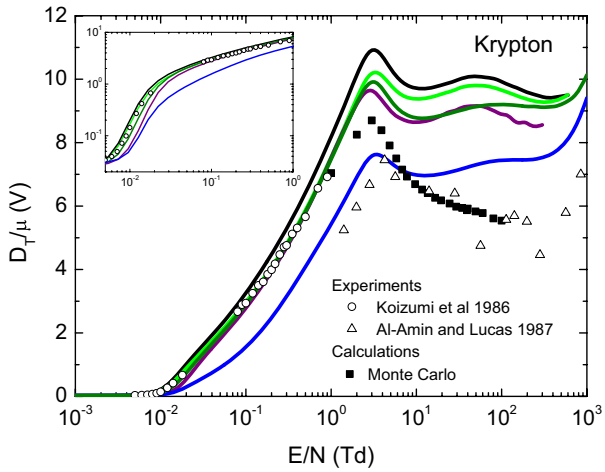

Figure 9. Measured and calculated D_T/μ versus E/N in krypton. The open symbols are experimental data referenced in the table 5. The lines are results from a two-term Boltzmann solver. The symbols (■) are for Monte Carlo calculations with BIAGI-v8.9 dataset. The inset shows results at low E/N. The color code is: BIAGI-v8.9 (——); BIAGI-v7.1 (——); BSR+ (——); SIGLO (——); MORGAN (——).

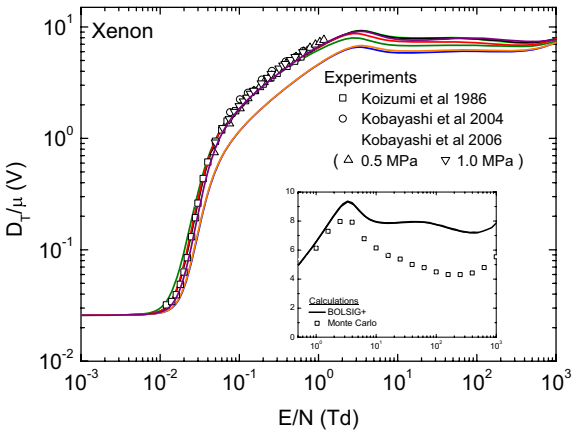

Figure 10. Measured and calculated D_T/μ versus E/N in xenon. The symbols are experimental data referenced in the table 5. The lines are results from two-term Boltzmann calculations. The inset shows comparisons between calculations using BIAGI-v8.9 dataset; the symbols (□) are for Monte Carlo calculations. The color code is: BIAGI-v8.9 (——); BIAGI-v7.1 (——); BSR+ (——); HAYASHI (——); SIGLO (——); MORGAN (——); PUECH (——).

(some 8%) at 230 Td. Some attempts were made to modify the xenon elastic cross section in the region between 5 and 20 eV in order to fit to the mobility above 100 Td. However all physically reasonable changes to the cross sections gave worse fits to the lower mobility data.

Both for krypton and for xenon, Monte Carlo calculations using BIAGI-v8.9 are in reasonable agreement with results from BOLSIG+ over the full range of values of E/N, with maximum differences in the reduced mobilities of about 8% for xenon at 500 Td for the spatial growth model (SST). It is interesting to note that there is better than 0.2% agreement between the Monte Carlo and BOLSIG+ mobilities calculated using the temporal growth model over the entire range of values of E/N.

3.2. D_T/μ and D_L/μ

Other commonly measured swarm data include D_T/μ and D_L/μ where D_T and D_L are the transverse and longitudinal diffusion coefficients, respectively. The transverse diffusion coefficient is very sensitive to the depth of the Ramsauer minimum, more so than the drift velocity; this is also true in the other Ramsauer noble gases, argon (paper I). The characteristic energy, u_k, is equal to eD_T/μ. The characteristic energy can be thought of as the potential energy through which an 'average' electron can diffuse against the electric field. Since the average electron energy is not easily accessible experimentally, the measured u_k provides a very useful energy scale even though there is no simple relation between average energy and u_k for realistic eedfs (Huxley and Crompton 1974).

The calculated D_T/μ versus E/N in krypton and xenon are shown in figures 9 and 10, respectively, over a range of E/N from 10^{-3} to about 1000 Td. These are shown for the different datasets discussed above and are compared with selected experimental data.

As mentioned in paper I, in the limit of zero electric field, the eedf tends to a Maxwellian distribution at the gas temperature T_g and the ratio D_T/μ obeys the Einstein relationship ($D_T/\mu = k_B T_g/e$), where k_B is the Boltzmann constant, as is seen well on the double log scale shown in figure 10. At low E/N, D_T/μ increases rapidly with E/N in both Kr and Xe until about 3 Td (the position of the knee in the curves for mobilities), at which point inelastic collisions start to influence the eedf, causing a rapid decrease in its high-energy tail.

There is a relatively good agreement between all calculations with experimental data up to about 1 Td with the exceptions of SIGLO (Kr and Xe) and PUECH (Xe). Note that for these datasets, the elastic momentum transfer cross sections at the Ramsauer minimum in each gas are larger than in the other data sets (see figures 1 and 2), and this reduces the D_T/μ for E/N below the knee at about 3 Td. For higher E/N, limited experimental data are available and these show large scatter (see figure 9).

We have compared the values of D_T/μ calculated with the two-term Boltzmann solver BOLSIG+ (Hagelaar and Pitchford 2005) and Monte Carlo codes (Biagi 2011, Hagelaar 2012) using the same BIAGI-v8.9 dataset for krypton and xenon as seen in figures 9 and 10. The two Monte Carlo codes give the same results. We find large differences between Monte Carlo and two-term Boltzmann results for D_T/μ for $E/N > 1$ Td in both gases, differences are as large as 40% in xenon at 100 Td. The Monte Carlo calculations in krypton are closer to the experimental data of Al-Amin and Lucas (1987) than are the two-term calculations using the same BIAGI-v8.9 dataset. Large differences between two-term and Monte Carlo calculations of D_T/μ are also found in argon (see figure 7 in paper I) but not in helium or neon where no Ramsauer minima are present. The size of the error induced by the two-term approximation becomes larger with the heavier gases which have deeper Ramsauer dips. We therefore ascribe the breakdown in the two-term approximation to be proportional

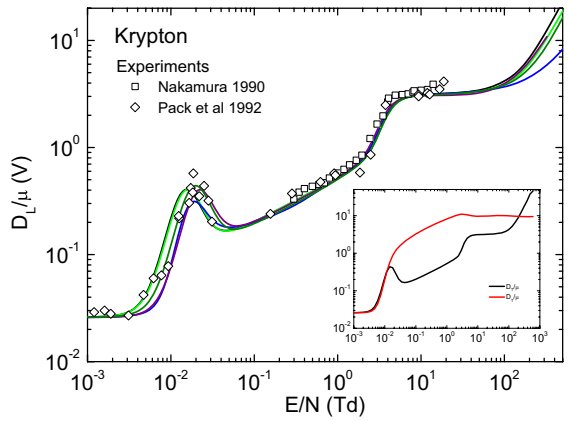

Figure 11. Calculated and measured D_L/μ versus E/N in krypton. The symbols are experimental data referenced in the table 5 and the lines are results from a two-term Boltzmann solver. The inset shows the comparison of D_T/μ and D_L/μ calculated using BIAGI-v8.9 dataset. The color code is: BIAGI-v8.9 (——); BIAGI-v7.1 (——); BSR+ (——); SIGLO (——); MORGAN (——).

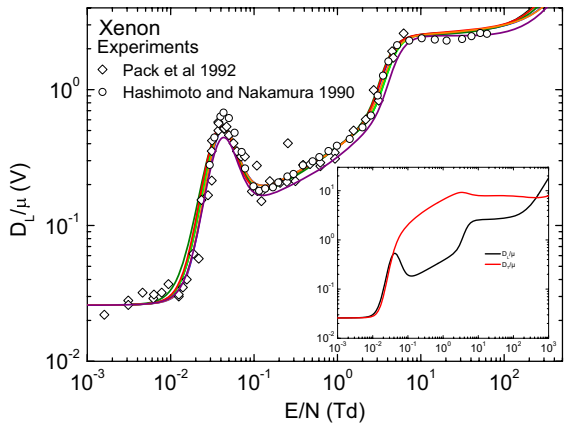

Figure 12. Calculated and measured D_L/μ versus E/N in xenon. The symbols are experimental data referenced in the table 5. The lines are results from a two-term Boltzmann solver. The inset shows the comparison of D_T/μ and D_L/μ calculated using BIAGI-v8.9 dataset. The color code is: BIAGI-v8.9 (——); BIAGI-v7.1 (——); BSR+ (——); HAYASHI (——); SIGLO (——); MORGAN (——); PUECH (——).

to the depth of the Ramsauer minimum and confirm this is true with test calculations.

Figures 11 (for krypton) and 12 (for xenon) compare calculations and measurements for the ratio of the longitudinal diffusion coefficient to the mobility, D_L/μ. The two quantities D_T/μ and D_L/μ can be very different at a given value of E/N (D_T/μ is much larger than D_L/μ over the whole E/N range analysed for these two gases), and the shape of D_T/μ varies considerably from the shape of D_L/μ (see insets in figures 11 and 12). The structure of the elastic momentum transfer cross sections has a direct bearing on the form of D_T/μ and D_L/μ, as functions of E/N. The D_L/μ curve exhibits a peak below 0.1 Td for the two studied gases, which occurs at an electron energy of the swarm corresponding to the steepest fall in the cross section before the Ramsauer minimum. The electrons in this energy range can have the widest spread in the scattering lengths, which contributes to an increase in the longitudinal diffusion coefficient. Conversely, when the

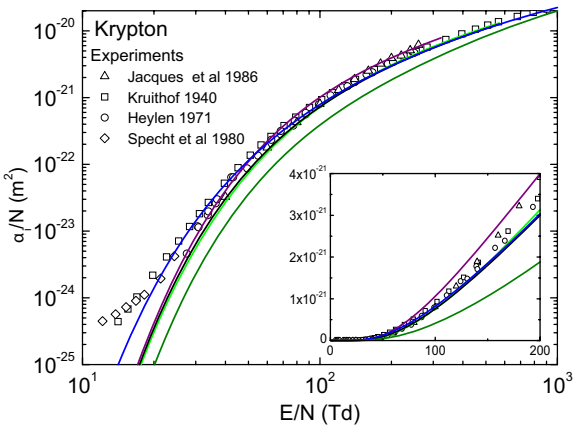

Figure 13. Calculated and measured reduced ionization coefficient versus E/N in krypton. The lines are results from two-term Boltzmann calculations and the symbols are experimental data referenced in the table 5. The inset is the same representation on a linear scale, to better illustrate the small differences in the calculations. The color code is: BIAGI-v8.9 (——); BIAGI-v7.1 (——); BSR+ (——); SIGLO (——); MORGAN (——).

electrons concentrate at the bottom of the Ramsauer dip the range of their scattering length reduces and a shallow minimum occurs, as seen in the D_L/μ plots (figures 11 and 12).

The two-term Boltzmann calculations reproduce reasonably well the shape of D_L/μ, with larger discrepancies in the location and the amplitude of its maximum, particularly for the different datasets with krypton. The calculated values of D_L/μ, whatever the method of calculation (two-term, multi-term or Monte Carlo simulation) are very close (differences <2% for $E/N < 100$ Td).

3.3. Reduced ionization coefficient

The calculations of the reduced ionization coefficient α_i/N as a function of E/N are shown in figures 13 and 14 for krypton and xenon, respectively, where experimental data are also compared. The insets on a linear scale serve to better illustrate the small differences in the calculations at E/N lower than 200 Td. Reliable values of the reduced ionization coefficient are crucial for fluid models of plasmas because this controls the ionization balance.

Since they have the lowest excitation threshold among the noble gases (8.315 eV for xenon and 9.915 eV for krypton), they are less sensitive than the other rare gases to Penning effects caused by impurities in the pure gas. Conversely they are more sensitive to Penning effects when used as the minority component of gas mixtures (for example Ne–Xe mixtures, Sakai *et al* 1991).

The BSR+ ionization calculations in krypton and xenon are low compared to experiment, probably because too much of the electron energy is deposited in the excitation of triplet levels, when using this dataset (see figures 3 and 4 for the total excitation cross sections in Kr and Xe). A similar result is observed for MORGAN in xenon, whose total excitation cross section is also larger than those for the other datasets at low energy (see figure 4), thus yielding smaller values for α_i/N. In krypton, at E/N lower than 100 Td, the reduced ionization

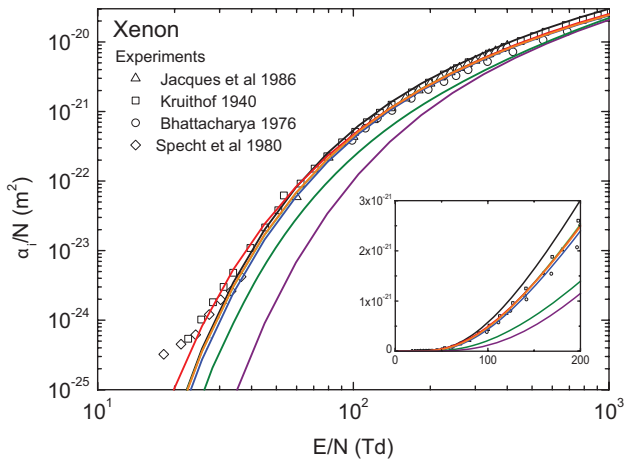

Figure 14. Calculated and measured reduced ionization coefficient versus E/N in xenon. The lines are results from two-term Boltzmann calculations and the symbols are experimental data referenced in the table 5. The inset is the same representation on a linear scale, to better illustrate the small differences in the calculations. The color code is: BIAGI-v8.9 (——); BIAGI-v7.1 (——); BSR+ (——); HAYASHI (——); SIGLO (——); MORGAN (——); PUECH (——).

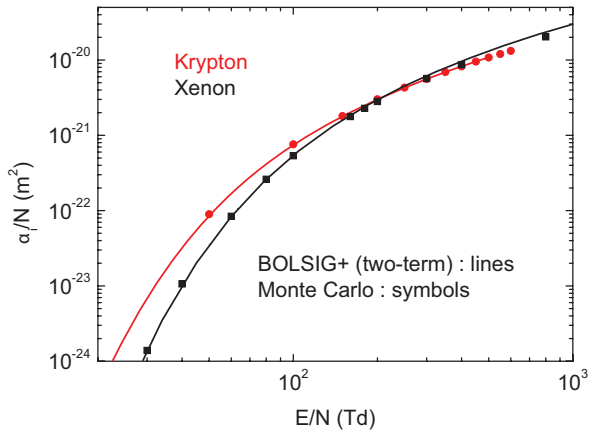

Figure 15. Calculations of the reduced ionization coefficient versus E/N in krypton (in red) and xenon (in black), obtained with a two-term Boltzmann solver and a Monte Carlo code using the BIAGI-v8.9 dataset.

coefficient calculated with BIAGI-v7.1 is slightly below that calculated with BIAGI-v8.9.

There is general agreement in the experimental data for α_i/N presented in figures 13 and 14 (deviations <40% for $E/N > 50$ Td). Notice, however, that the results of Specht *et al* (1980) are contaminated by secondary processes, such as the Penning ionization of impurities and the emission of electrons from the cathode caused by the photoelectric effect or the impact of ions. Thus, the resulting *total* ionization coefficient should be corrected for these phenomena, so as to consider only the *direct* ionization coefficient in our comparisons.

Figures 13 and 14 show a general trend of calculated ionization coefficients at low E/N being below the experimental values. This trend is even more pronounced in the other noble gases with higher ionization potentials; we ascribe the general behaviour to the experimental measurements having a contribution from Penning ionization of impurities which explains the large effect seen at low values of E/N.

The two-term approximation yields accurate results for α_i/N in Kr and Xe, when compared to Monte Carlo simulations, as shown in figure 15 (differences lower than 1% at 500 Td for xenon).

4. Recommendations and conclusions

We have compared the electron scattering cross sections from ground-state atoms, available on the open-access LXCat website for krypton (five datasets) and for xenon (seven datasets). The comparison focused on the elastic momentum transfer cross section, for which general good agreement between the different datasets was found, and on the total excitation cross section, where major differences (for example, in krypton at the maximum, they can be of the order a factor 3) were observed. The datasets are very different in the level of detail, but when possible individual excitation cross sections were also compared. In general, the cross sections with the various sets were determined so as to reproduce measured swarm parameters, with the exception of BSR, obtained from *ab initio* quantum mechanical calculations for elastic and excitation events only.

All datasets were used to calculate swarm parameters (reduced mobility, characteristic energy, reduced longitudinal diffusion coefficient and reduced ionization coefficient) over a large E/N range, using a two-term Boltzmann equation solver (BOLSIG+). Two independently developed Monte Carlo codes (MAGBOLTZ and MCIG) and a multi-term Boltzmann solver (Ségur *et al* 1984) were used to check the accuracy of the faster and more flexible two-term Boltzmann calculations. In these calculations, the (incomplete) BSR datasets were converted into BSR+, by including accurately measured ionization cross sections for krypton and xenon. The calculated results were compared with available experimental swarm data, to assess the consistency of the cross sections sets with measurements.

Both BIAGI datasets and the HAYASHI dataset are consistent with experimental swarm data in krypton and xenon over a wide range of values of E/N. The PUECH and SIGLO datasets yield good results for reduced mobility and the reduced ionization coefficient, critically important for plasma modelling, but they are inconsistent with the measured values of D_T/μ at low fields in Kr (SIGLO) and Xe (SIGLO and PUECH) probably because the cross sections for elastic momentum transfer in these datasets are too high in the region of the Ramsauer minima. Adjustment could be made to improve the agreement, but this is not the point of the present paper. MORGAN results for the transport parameters at E/N values higher than a few Townsend deviate from experimental results more than do the results from the other datasets. This is apparently due to the limited energy range of its elastic momentum transfer cross section, especially in xenon. The other more recently compiled datasets are to be preferred for both krypton and xenon.

BSR+ calculations are also in relatively good agreement with experiment, except for the reduced ionization coefficient.

As discussed in Papers I and II for argon and neon, respectively, theoretical cross sections in those two cases have reached the point of being able to provide complete sets of cross sections suitable for calculations of swarm parameters. More work is needed to reach this point for the heavier rare gases, as is described in appendix B.

For pure noble gases with Ramsauer-Townsend minimum, the two-term calculations give accurate values of μN, D_L/μ and α_i/N, and also of D_T/μ at E/Nlower than about 1 Td. However, if accurate values of the characteristic energy are required at higher E/N, it should be noted that the two-term approximation can introduce large errors (40% in xenon at 100 Td).

The analysis carried out in this work lets us identify several difficulties and needs in the calculation of accurate swarm data. As described in appendix E for the krypton dataset with SIGLO, the error introduced by digitization of cross section data from published figures can seriously compromise the comparisons of calculated and measured swarm parameters. We strongly recommend that cross section data be made available in the form of tables to eliminate sources of error due to digitization.

We take this opportunity to recommend some experimental measurements that would improve the accuracy of the extraction of cross sections and remove ambiguities.

- The Ramsauer minimum position and cross section could be determined more precisely if the measurements of the drift velocity in the region of the mobility maximum, 0.01 to 0.1 Td, were repeated with both krypton and xenon ultra-pure gases and systematic errors of less than $\pm 1\%$. The experiment should also measure the longitudinal diffusion which displays a peak at the same field although this serves as a check and does not constrain the cross sections as well as a high accuracy drift velocity measurement.
- Precision data is also lacking for the mobility (drift velocity) above about 50 Td in both Kr and Xe. In this region, the drift velocity is sensitive to the peak of the elastic momentum transfer cross section. More guidance from experiment is needed here and an experimental accuracy of 2% would be adequate at this high field.
- There is a large spread in the experimental measurements of the ionization coefficient in krypton; accurate measurements in pure krypton would be desirable although less important than xenon which has many uses in other fields such as light sources and radiation detectors.
- Data are missing for describing the excitation to individual states, particularly in heavy noble gases.

These are only some examples where more guidance from experiment is needed to improve the quality of collisional data and of predictions of transport parameters and rate coefficients for plasma modelling.

Acknowledgments

The authors gratefully acknowledge the Gaseous Electronics Conference for having established the PDED. The work of OZ and KB was supported by the United States National Science Foundation under grants PHY-1068140 and PHY-1212450, and by the XSEDE supercomputer allocation PHY-090031. The work of LLA was partially supported by Fundação para a Ciência e a Tecnologia, under Project Pest OE/SADG/LA0010/2011.

Appendix A. Comments on BIAGI-v7.1 and BIAGI-v8.9 databases (by SF Biagi)

The cross section sets for krypton and xenon in BIAGI-v7.1 and BIAGI-v8.9 were derived in 2003 and 2010 respectively. The experimental and theoretical inputs to the data sets were updated from the literature with these cutoff dates. The 8.9 data set involved a more detailed description of the level structure in the atoms in order to accurately predict the light emission from avalanches in the gases used in radiation detectors. Extensive use was made of BE-f (Kim 2001) scaling using the latest oscillator strengths of dipole allowed levels in the 8.97 update. The BSR predictions of the resonance structure close to threshold was extensively used for the s-levels. The triplet states cross sections were chosen to agree with the Jet Propulsion Laboratory measurements (Khakoo *et al* 1994, 1996a, 1996b), where available, within experimental error and scaled to fit the ionization coefficient measurements.

The ionization cross sections were taken for krypton from the weighted average of the measurements of Rapp and Englander-Golden (1965) and Lindsay (Rejoub *et al* 2002) and RICE website: www.ruf.rice.edu/~atmol/electron_ data.html since they were in agreement. However, the xenon ionization cross section was not consistent between the above two accurate datasets. On closer reading the Rapp and Englander-Golden data set was acknowledged in the publication to have problems with the gas pressure measurements which proved to be inconsistent. The gas pressure in the measurement technique gives the overall normalization of the cross sections and is the largest contribution to the measurement error. In the xenon analysis we therefore used the Lindsay value of the ionization cross section at the peak at 125 eV. The Rapp and Englander-Golden data set was then renormalized to this peak value and the average taken of the two data sets which then agreed within errors. A further small correction was made to the Rapp and Englander-Golden data set below 30 eV. This correction was justified since there was a kink in the smooth shape of the cross section at this energy where two different pressures were used in the Rapp and Englander-Golden measurements. These modifications lead to good agreement with the gain measured in proportional detectors and formed a consistent set with the 8.9 excitation cross sections.

The elastic momentum transfer cross section in krypton and xenon at energies below 3 eV was taken from the analysis of Elford (2002) and extended to higher energy by fitting to the available drift velocity and diffusion coefficients. The ionization coefficient was then fitted by scaling the triplet excitation cross sections for both krypton and xenon.

Appendix B. Comments on the BSR database (by K Bartschat)

The Dirac B-spline R-matrix (DBSR) results originate from the work described by Zatsarinny *et al* (2011) (e–Kr elastic), Allan *et al* (2011) (e–Kr inelastic), and Zatsarinny and Bartschat (2010) (e–Kr and e–Xe). The calculations are based on the fully *ab initio*, non-perturbative close-coupling expansion for the projectile + target collision system. Relativistic effects were accounted for at the level of the fully relativistic Dirac-Coulomb approach. The DBSR method was described in detail by Zatsarinny and Bartschat (2008). A newly developed (not yet published) code was employed to solve the resulting equations. This code is the fully relativistic companion of the Breit-Pauli suite of computer codes described by Zatsarinny (2006). For more information about general theoretical methods for electron–atom collisions, we refer to the paper written by Bartschat (2013) as part of this series.

The respective close-coupling expansions for *excitation* contained at least the lowest 31 (27) physical states of Kr (Xe). For Kr, these are the ground state with dominant configuration $(4p^6)\,^1S_0$ and the excited states with dominant configurations $4p^5 5s$ (four states), $4p^5 5p$ (ten states), $4p^5 4d$ (twelve states), and $4p^5 6s$ (five states), respectively. In the Xe case, the principal quantum numbers of the above configurations are essentially increased by one. In order to accurately describe near-threshold excitation of the lowest few inelastic states, it was deemed important to include several more Rydberg states in the calculation. Due to the large splitting of the ionic $(5p^5)\,^2P_{3/2}$ and $(5p^5)2P_{1/2}$ cores, most of the higher bound states for Xe had a $^2P_{3/2}$ core (Zatsarinny and Bartschat 2010). The close-coupling expansions for the e–Kr and e–Xe excitation cross sections currently in LXCat contained 69 and 75 states, respectively.

For *elastic* scattering, on the other hand, a different approach was chosen. Here a single 'pseudo-state' with total electronic angular momentum $J = 1$ was generated in order to ensure a good representation of the dipole polarizability of the ground state. This is known to be of critical importance for a proper description of the Ramsauer-Townsend minimum in the low-energy elastic regime. Although being only a 2-state model, the agreement with experimental benchmark data obtained with it is excellent (Zatsarinny *et al* 2011).

The BSR cross sections in the current LXCat database are the best we can currently produce with our approach. As mentioned above, these quantum mechanical calculations are fully *ab initio*, except for minor adjustments (at the 0.2 eV level in Xe and less in Kr) to the theoretically predicted excitation energies of the various states. Using experimental thresholds allows for a straightforward comparison of experiment and theory in the near-threshold resonance region. For practical applications such as those discussed in the present paper, however, these adjustments have no appreciable effect on the results.

Based on detailed comparisons between experimental data for state-resolved, highly differential (in energy and angle) observables, as well as the experience gained on this type of calculations over many years, we can make some general statements about the likely accuracy of the BSR predictions. Specifically:

- We believe the elastic and momentum transfer cross sections to be accurate at the 10 percent level. This assessment is supported by the good agreement seen in this paper between modelling predictions using these cross sections and the corresponding experimental data (where applicable, i.e. for cases for which ionization is not of critical importance).
- The excitation results, especially for incident projectile energies above the ionization threshold and for weak, optically forbidden transitions, are expected to generally overestimate the true cross sections. The reason for the problem is the fact that possibly important coupling to the ionization continuum, and to a smaller extent also to the even higher-lying Rydberg states, is omitted in the current models that only couple physical bound states. Our experience suggests that close-coupling, as a unitary theory that conserves the total flux, will try to simulate processes such as ionization by (incorrectly) redistributing the corresponding flux into the excitation channels. See also paper IV (Bartschat 2013).
- The problem was analysed in two recent publications (Zatsarinny *et al* 2012a, 2012b) on e–Ne collisions. In that work, the close-coupling expansion was extended significantly by including so-called 'pseudo-states'. These short-range states with a discrete energy spectrum serve as a numerical discretization of the target continuum and a coarse sampling of the high-lying Rydberg states. Results from those calculations for e–Ne and e–Ar are already in the LXCat database and will be presented in the adjacent papers on electron collision data for helium and neon (paper II) as well as argon (paper I). Performing similar large-scale calculations for e–Kr and even e–Xe is, in principle, possible, but for us currently only in the semi-relativistic approach. At this point, however, our focus is on extending the Dirac-Coulomb DBSR code to a fully parallelized version that will, ultimately, be preferable.

Realistically, BSR results from such calculations should not be expected until a few years from now. Until they become available, we cannot predict the ionization cross section, and it is also virtually impossible to provide a reliable estimate regarding the accuracy of the excitation results. As mentioned above, it is highly likely that we are overestimating the true excitation cross sections in the 'intermediate energy' regime between the ionization threshold and a few times that energy. Given that the effect is less dramatic in Ar compared to Ne, and that the models from which we obtain the excitation cross sections contain more than 31 bound states, we expect the results for e–Kr and e–Xe to be relatively better than the early 31-state results for e–Ne (Zatsarinny and Bartschat 2004a) and e–Ar (Zatsarinny and Bartschat 2004b), which were recently replaced in LXCat by the large-scale pseudo-state results.

Appendix C. Comments on the HAYASHI database (by LC Pitchford and AV Phelps)

Professor Makoto Hayashi compiled bibliographies and recommended data sets for a number of gases and reported

some these in a book chapter (Hayashi 1987) and in a series of reports from the National Institute For Fusion Science in Japan. These summarize results from his compilations of data undertaken while he was at Nagoya Institute of Technology and, after his retirement, at Gaseous Electronics Institute in Nagoya. The NIFS reports are available online at www.nifs.ac.jp/report/nifsdata.html. A separate database on LXCat was set up so as to include this trove of data from Hayashi in the Plasma Data Exchange Project. The xenon data discussed in the present paper are available in tabular form at the end of the Hayashi's 2003 NIFS report on xenon (Hayashi 2003). His recommended cross sections in xenon are dated 1990, and are considerably more detailed than his previous dataset for xenon (Hayashi 1983). In (Hayashi 1987), he states that his cross sections datasets were 'determined from available data from electron beam and electron swarm experiments via the Boltzmann equation and the Monte Carlo simulation method. The beam data were given highest priority, and theoretical values of cross sections were sometimes used'.

Appendix D. Comments on the PUECH database

The paper by Puech and Mizzi (1991) describes in detail the procedure used for the compilation and validation of this xenon cross section set.

Appendix E. Comments on SIGLO database (by LC Pitchford)

The SIGLO database is a collection of sets of cross sections for electron scattering in various gases. This collection has been compiled over the course of 20 years by students, post-docs and researchers in the group GREPHE at LAPLACE in Toulouse, France.

Appendix E.1. Krypton

The cross sections for Krypton in the SIGLO database were digitized from figures 1 and 5 of Date *et al* (1989). This cross section set includes momentum transfer, five inelastic and one ionization processes. The momentum transfer cross section is derived from different authors and is presumably an elastic rather than total momentum transfer cross section because it drops below the ionization and excitation cross sections for energies less than 100 eV (the maximum energy in the figures). The excitation levels correspond to $1s_5$, $1s_4$, $1s_3$, and $1s_2$ (identified by Date *et al* in LS notation as $^3P_2$, $^3P_1$, $^3P_0$ and $^1P_1$) with one additional 'lumped' level which is intended to represent the sum of all other excitation processes. The thresholds (energy losses) for these states are 9.915 eV, 10.032 eV, 10.562 eV, 10.644 eV, and 11.304 eV, respectively, for the 4 lower levels and the lumped level. The latter corresponds to the threshold energy for the next lowest excited state ($2p^{10}$). Date *et al* base their cross sections for excitation to these levels on Trajmar *et al* (1981) and the ionization cross section is taken from Rapp and Englander-Golden (1965).

Date *et al* find good agreement between measured and calculated drift velocity and ionization coefficients versus E/N when using their cross section set in a two-term Boltzmann solver. They point out that there are several sets of measurements for the ionization coefficients and that with a slight modification in the low-energy part of the cross section for excitation of the lumped level, they can get good agreement with one or the other of the measured curves for ionization coefficient versus E/N. We have retained the data in curve A in their figure 5 for the lumped level excitation cross section in an attempt to reproduce the good agreement found by Date *et al* with the experimental results of Kruithof (1940) and Heylen (1971) rather than their curve B (figure 5) which gives better agreement with the measurements of Dutton *et al* (1983).

During the course of this evaluation effort, we re-digitized the data from this reference and corrected slightly the threshold energies for each level. These updates (updated on LXCat in Nov 2012) led to better somewhat agreement with the swarm parameters. However, our assessment is that our digitization procedure does not have the precision required to accurately reproduce the cross sections in the publication. We have chosen to leave these data for krypton on the SIGLO database for the moment. Comments available on the LXCat site provide a detailed history of the available data. We note in particular that we re-digitized the data from Date *et al* and replaced the data previously available on SIGLO with the newly digitized data in November 2012.

Appendix E.2. Xenon

The xenon dataset was assembled by Meunier *et al* (1995) for their work on modelling plasma display panel cells in Ne/Xe mixtures. The multi-term code of Ségur *et al* (1984) and the Monte Carlo code of Boeuf and Marode (1982) were used to calculate the transport and rate coefficients in neon/xenon mixtures using the cross section data in the SIGLO database, and these transport and rate coefficient data were then used in the fluid model of presented in Meunier *et al* (1995). The calculated reduced ionization coefficients and reduced electron mobilities in pure xenon are in reasonable agreement with experiment. For the purposes of the model, the characteristic energy was assumed to be 1 eV and so a calculation of diffusion coefficients was not done. These data for xenon were included in the input data files distributed with the freeware packages BOLSIG (Pitchford *et al* 1996) and BOLSIG+ (Hagelaar and Pitchford 2005).

The elastic momentum transfer cross section was taken from Hunter *et al* (1988) at low energy and from Hayashi (1983) at higher energies. Excitation to the following levels of groups of levels are included in the SIGLO xenon dataset: (1) $1s_5$ metastable level, (2) $1s_4$ resonance level, (3) $1s_2$, $1s_3$ and the five lower 2p levels, (4) 2s and 3d levels, (4), higher five 2p levels, (5) all higher levels. The excitation cross sections were based on the compilation of Puech and Mizzi (1991). The ionization cross sections are from Rapp and Englander-Golden (1965). Although not part of the discussion in this paper, the cross sections included in the SIGLO database on LXCat for ionization of the metastable levels of neon and xenon are from Thon-That and Flannery (1977).

References

Al-Amin S A J and Lucas J 1987 *J. Phys. D: Appl. Phys.* **20** 1590

Allan M, Zatsarinny O and Bartschat K 2011 *J. Phys. B: At. Mol. Opt. Phys.* **44** 065201

Alves L L, Bartschat K, Biagi S F, Bordage M C, Pitchford L C, Ferreira C M, Hagelaar G J M, Morgan W L, Pancheshnyi S, Phelps A V, Puech V and Zatsarinny O *et al* 2013 *J. Phys. D: Appl. Phys.* **46** 334002

Bartschat K 2013 *J. Phys. D: Appl. Phys.* **46** 334004

Bhattacharya A K 1976 *Phys. Rev.* A **13** 1219

Becker K H, Kogelschatz U, Schoenbach K H and Barker R J 2005 *Non-Equilibrium Air Plasmas at Atmospheric Pressure* (Bristol: Institute of Physics Publishing)

Biagi S F 2011 Fortran Monte Carlo code MAGBOLTZ, version 8.97 and http://consult.cern.ch/writeup/magboltz

BOLSIG+ www.bolsig.laplace.univ-tlse.fr Note that the online Boltzmann solver available on LXCat website is intented to give users a quick estimates of swarm parameters in pure gases and in gas mixtures where cross section data for the components of the mixture are available on LXCat. For detailed calculations the download version should be used because of its greater flexibility.

Boeuf J P and Marode E 1982 *J. Phys. D: Appl. Phys.* **15** 2169

Boeuf J P 2003 *J. Phys. D: Appl. Phys.* **36** R53

Bordage M C, Hagelaar G J M, Pitchford L C, Biagi S F and Puech V 2011 *64th Gaseous Electronics Conf. (Salt Lake City, UT)* p 56

Date H, Sakai Y and Tagashira H 1989 *J. Phys. D: Appl. Phys.* **22** 1478

Dutton J 1975 *J. Phys. Chem. Ref. Data* **4** 577

Dutton J, Mat Yunus W M and Williams A W 1983 *Proc. 16th ICPIG (Düsseldorf, Germany)* vol 2 (Henkel) p 158

Elford M T 2002 private communication

Hagelaar G J M and Pitchford L C 2005 *Plasma Sources Sci. Technol.* **14** 722

Hagelaar G J M 2012 MCIG: Monte Carlo for Ionized Gases, unpublished Monte Carlo code, private communication

Hayashi M 1987 *Swarm Studies and Inelastic Electron–Molecule Collisions* ed L C Pitchford *et al* (Berlin: Springer)

Hayashi M 1983 *J. Phys. D: Appl. Phys.* **16** 581

Hayashi M 2003 Japanese National Institute for Fusion Science *NIFS-DATA-79 Report*

Hashimoto T and Nakamura Y 1990 Paper of *Gas Discharge Technical Commitee (IEE Japan, Tokyo)* ED-90-61

Heylen A E D 1971 *Int. J. Electron.* **31** 19

Hoffmann T H, Ruf M-W, Hotop H, Zatsarinny O, Bartschat K and Allan M 2010 *J. Phys. B: At. Mol. Opt. Phys.* **43** 085206

Hunter S R, Carter J G and Christophorou L G 1988 *Phys. Rev.* A **38** 5539

Huxley L G H and Crompton R W 1974 *The Diffusion and Drift of Electrons in Gases* (New York: Wiley-interscience)

Jacques L, Bruynooghe W, Boucique R and Wieme W 1986 *J. Phys. D: Appl. Phys.* **19** 1731

Kim Y K 2001 *Phys. Rev.* A **64** 032713

Khakoo M A, Beckmann C E, Trajmar S and Csanak G 1994 *J. Phys. B: At. Mol. Opt. Phys.* **27** 3159

Khakoo M A, Trajmar S, Leclair L R, Kanik I, Csanak G and Fontes C J 1996a *J. Phys. B: At. Mol. Opt. Phys.* **29** 3455

Khakoo M A, Trajmar S, Wang S, Kanik I, Aguirre A, Fontes C J, Clark R E H and Abdallah J 1996b *J. Phys. B: At. Mol. Opt. Phys.* **29** 3477

Kobayashi S, Hasebe N, Igarashi T, Miyachi T, Miyajima M, Okada H, Doke T, Shibamura E, Dmitrenko V V and Vlasik K F 2004 *Japan. J. Appl. Phys.* **43** 5568

Kobayashi S *et al* 2006 *Japan. J. Appl. Phys.* **45** 7894

Kogelschatz U, Eliasson B and Egli W 1997 *Invited Paper, 23rd ICPIG (Toulouse, France) J. de Physique IV* **7** C4/47

Koizumi T, Shirakawa E and Ogawa I 1986 *J. Phys. B: At. Mol. Opt. Phys.* **19** 2331

Kowari K, Kimura M and Inokuti M 1989 *Phys. Rev.* A **39** 5545

Kramida A, Ralchenko Y and Reader J 2013 *NIST Atomic Spectra Database* and www.nist.gov/pml/data/asd.cfm

Kruithof A A 1940 *Physica* **7** 519

Kücükarpaci H N and Lucas J 1981 *J. Phys. D: Appl. Phys.* **14** 2001

Laroussi M, Dobbs F C, Wei Z, Doblin M A, Ball L G, Moreira K R and Dyer F F 2002 *IEEE Trans. Plasma Sci.* **30** 1501

Meunier J, Belenguer Ph and Boeuf J P 1995 *J. Appl. Phys.* **78** 731

Morgan W L and Penetrante B M 1990 *Comput. Phys. Commun.* **58** 127

Nakamura Y 1990 *Non Equilibrium Effects in Ion and Electron Transport* ed J W Gallagher *et al* (Berlin: Springer) US 10.1007/978-1-4613-0661-0_33 363

Okhrimovskyy A, Bogaerts A and Gijbels R 2002 *Phys. Rev.* E **65** 032713

Pack J L, Voshall R E, Phelps A V and Kline L E 1992 *J. Appl. Phys.* **71** 5363

Pancheshny S, Biagi S F, Bordage M C, Hagelaar G J M, Morgan W L, Phelps A V and Pitchford L C 2012 *Chem. Phys.* **398** 148

Phelps A V and Pitchford L C 1985 *Phys. Rev.* A **31** 2932

Pitchford L C, Boeuf J P and Morgan W L 1996 *23rd IEEE Int. Conf. on Plasma Science (Boston, MA)*

Pitchford L C, Alves L L, Bartschat K, Biagi S F, Bordage M C, Phelps A V, Ferreira C M, Hagelaar G J M, Morgan W L, Pancheshnyi S, Puech V, Stauffer A and Zatsarinny O 2013 *J. Phys. D: Appl. Phys.* **46** 334001

Puech V and Mizzi S 1991 *J. Phys. D: Appl. Phys.* **24** 1974

Rapp D and Englander-Golden P 1965 *J. Chem. Phys.* **43** 1464

Rejoub R, Lindsay B G and Stebbings R F 2002 *Phys. Rev.* A **65** 042713

Rhodes C K 1979 *Excimer Lasers*, Ed C K Rhodes, Springer Verlab, Berlin

Sakai Y, Sawada S and Tagashira H 1991 *J. Phys. D: Appl. Phys.* **24** 283

Santos F P, Dias T H, Stauffer A D and Conde C A N 1991 *Nucl. Instrum. Methods* A **307** 346

Šašić O, Jovanović J, Petrović Z Lj, de Urquijo J, Castrejón-Pita J R, Hernández-Ávila J L and Basutro E 2005 *Phys Rev* E **71** 046408

Segur P, Yousfi M, and Bordage M C 1984 *J. Phys. D: Appl. Phys.* **17** 2199

Segur P, Yousfi M, Kadri M and Bordage M C 1986 *Trans. Theory Stat. Phys.* **15** 705

Sosnin E A, Oppenlander T and Tarasenko V F 2006 *J. Photochem. Photobiol.* C **7** 145

Specht L T, Lawton S A and deTemple T A 1980 *J. Appl. Phys.* **51** 166

Thon-That D and Flannery M R 1977 *Phys. Rev.* A **15** 517

Trajmar S, Srivastava S K, Tanaka H and Nishimura H 1981 *Phys. Rev.* A **23** 2167

Waibel E and Grosswendt B 1991 *Nucl. Instrum. Methods* B **53** 239

Wetzel R C, Baiocchi F A, Hayes T R and Freund R S 1987 *Phys. Rev.* A **35** 559

Zatsarinny O and Bartschat K 2004a *J. Phys. B: At. Mol. Opt. Phys.* **37** 2173

Zatsarinny O and Bartschat K 2004b *J. Phys. B: At. Mol. Opt. Phys.* **37** 4693

Zatsarinny O 2006 *Comput. Phys. Commun.* **174** 273

Zatsarinny O and Bartschat K 2008 *Phys. Rev.* A **77** 062701

Zatsarinny O and Bartschat K 2010 *J. Phys. B: At. Mol. Opt. Phys.* **43** 074031

Zatsarinny O, Bartschat K and Allan M 2011 *Phys. Rev.* A **83** 032713

Zatsarinny O and Bartschat K 2012a *Phys. Rev.* A **85** 062709

Zatsarinny O and Bartschat K 2012b *Phys. Rev.* A **86** 022717